J. Indian Inst. Sci., Jan.–Feb. 1998, **78**, 3–16.

Directional image analysis with the Hough and Radon transforms

RANGARAJ M. RANGAYYAN[1] AND WILLIAM A. ROLSTON[1,2]
[1]Department of Electrical and Computer Engineering, The University of Calgary, Calgary, Alberta, Canada, T2N1N4
[2]At present with Valmet Automation, Calgary, Canada

Abstract

The objective of the method to be developed in this paper is to obtain quantitative information on the directional distribution of features in a given image. The Hough transform can be regarded as a method of transforming an image into a domain that reduces the image into a set of parameters from which it is easier to obtain the desired information in the image. The main drawback of the Hough transform is that it is usually performed on binary images, and is thus dependent on the binarisation method that is used in segmenting the image. The implementation proposed in this paper avoids this drawback by designing a modified version of the Hough transform that uses concepts from the Radon transform to obtain a Hough/Radon transform.

In the proposed algorithm, the image is first transformed into the Hough/Radon domain, while at the same time a second shadow domain is created to keep count of the number of pixels at a particular parameter point. The Hough/Radon-transformed image is then filtered to obtain coherent peaks. The shadow parameter space is then integrated to obtain a count of the number of pixels corresponding to directional features in each angle band. Due to the summing of intensities in the Radon transform step, the algorithm detects directional elements on the basis of orientation as well as intensity.

Results with a set of six test images with various types of directional features indicate that the method can perform well over a reasonable range of feature types.

1. Introduction

In many instances of natural and man-made materials, strength is derived from the existence of highly coherent, oriented fibres; examples of such structure are found in ligaments[1–4] and paper and textiles[5–10]. Similar patterns exist in other biological tissues such as bones, muscle fibers, and blood vessels in ligaments as well[11–22]. Analysis of directional distribution of component fibres or the relevant basic material in such cases could provide useful information on the strength or state of health of the material or tissue.

Directional features exist in many other applications of imaging, and directional image filtering or processing techniques have been developed for a wide variety of applications. Directional or fan filters have been used extensively to filter seismic stacks[23–25]. Directional analysis could also be used in effective identification and segmentation of texture[26]. Other applications reported include analysis of LANDSAT maps for the detection of anomalies in map data[27–32]; identification of ancient river beds from satellite images[27]; identification of buildings and small urban features[31]; and dividing the frequency space into directional bands for efficient image coding[33–39].

Fourier methods have dominated the directional image processing scene[1,11,23,24,25]. Other approaches which have been followed are: numerical and statistical characterisation of directional "strength"[14]; morphological operations using a rotating structural element[22]; skeletonisation followed by line-fitting[17,18]; laser small-angle light scattering[10,19,20]; and optical diffraction and Fourier transform analysis[9,11,28,36].

The Hough transform is a powerful tool for analysis of features which may be parameterised, such as straight lines and circles[40–44]. While the Hough transform may be used to detect and analyse the orientation of straight lines, its use for complete and objective characterisation of the directional distribution or scatter in grey-scale images has not been explored. In this paper we propose a combination of the Hough transform with the Radon transform to overcome some limitations of the former, and study the effectiveness of the combined method with a few test patterns[45].

2. The Hough Transform

Quite often, it is convenient to transform the image being processed to another domain. Patterns that are not apparent in the image domain are sometimes easily identifiable in the transform domain. The Hough transform is a method for detecting curves that can be described by a number of parameters, such as lines, circles, and parabolas. The Hough transform has been used in pattern recognition[40–44] and for the detection of texture elements[46]. The Hough transform may be used to compute the locus, in a parameter space, of the set of curves passing through a point in the image plane.

Line segments can be completely characterised using the expression $y = mx + b$ where x and y represent arbitrary points in the (x, y) image plane, m is the slope, and b is the intercept of the line with the y axis. If, on the other hand, we assume that the (x, y) point is fixed, we have a two-dimensional (2D) space with the parameters m and b. A problem with this parameterisation is that both of the parameters (m, b) are unbounded. Through a re-parameterisation of these elements we can obtain a bounded parameter set.

From figure 1 we can see that a line can be specified by its orientation with respect to the x axis (θ) and its radial distance from the origin (ρ). From this parameterisation, we can see that any line is bounded in angular orientation to the interval $[0, \pi]$ and bound by the Euclidean distance to the farthest point of the image from the centre of the image. The equation for an arbitrary line segment in the image plane is then

$$\rho_o = x \cos \theta_o + y \sin \theta_o. \tag{1}$$

For a specific point in the image domain (x_i, y_i), we obtain a sinusoidal curve in the Hough transform domain. Each point (x_i, y_i) lying on a straight line with $\rho = \rho_0$ and $\theta = \theta_0$ in the image domain corresponds to a sinusoidal curve in the (ρ, θ) domain specified by

$$\rho = x_i \cos \theta + y_i \sin \theta. \tag{2}$$

Through equation 2 we see that for each point in the image domain, the Hough transform performs a one-to-many mapping to a modulated sum of sinusoids in the Hough domain. All of the sinusoids resulting from a mapping of a line in the image domain have a common point of

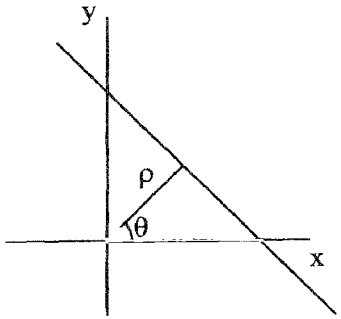

FIG 1. The normal parameters of a line.

intersection (ρ_0, θ_0) in the Hough domain. Thus, linear segments in the spatial domain correspond to large-valued points in the Hough domain.

The following statements summarise the properties of the Hough transform:

Property 1. A point in the image domain corresponds to a sinusoidal curve in the (ρ, θ) transform domain.

Property 2. A point in the (ρ, θ) transform domain corresponds to a straight line in the image domain.

Property 3. Points on the same curve in the (ρ, θ) transform domain correspond to lines through the same point in the image domain.

Property 4. Points on the same line in the image domain correspond to curves through the same point in the (ρ, θ) transform domain.

From the properties listed above, the Hough transform appears to be ideal for detecting linear components in images. However, there are some limitations to this approach. The results are sensitive to the quantisation intervals used for the angle θ and the distance ρ. Decreasing the quantisation step for θ increases the computation time since the calculation for ρ is typically done across each value of θ and each pixel. Another problem with this method is the "crosstalk" between lines in the Hough domain. For example, if an image contains several lines parallel to the x axis, they would correspond to several peak values in the Hough domain at differing ρ along the 0° line. However, the Hough transform also detects linear segments at 90°, which would show up as smaller peaks at a continuum of ρ values in the Hough domain. This is caused by the fact that the Hough transform finds line segments at specific ρ values that are not necessarily contiguous.

In the directional analysis method to be developed in this paper, we will use property 2 of the Hough transform which states that a point in the (ρ, θ) domain corresponds to a straight line

in the image domain. Through use of this property it is possible to obtain the directional nature of an image by integrating along one angle θ_i in the Hough transform domain to find the distribution of directional components that lie along this angle.

From equation 2 we can see that the Hough transform can be interpreted as a one-to-many mapping of a point from the image domain, specified by (x_i, y_i), to a set of points in the parameter domain, specified by (ρ, θ). This represents calculating the parameters of straight lines that pass through a given point (x_i, y_i). Each point in the image domain forms a sinusoid in the parameter domain, and points that are collinear in the image domain all intersect at a common point in the parameter space. This parameter point characterises the straight line connecting the constituent image points. Thus the Hough transform is often referred to as a "voting" procedure where each point in the image "votes" for all parameter combinations that could have produced it. We can use this fact to determine the directional content in an image since each point that is a member of the desired directional component will have only one vote characterised by one sinusoid in the parameter domain. The problem of determining the directional content of an image thus becomes a problem of peak detection in the parameter space. If we are able to select the peak in the parameter space which corresponds to the desired directional component in an image, we will be able to obtain all the pixels that compose that directional component.

The Hough transform has the desirable feature that it handles occlusion of directional components gracefully since the size of the parameter peaks is directly proportional to the number of matching points of the component. This last fact can also be a partial drawback due to "crosstalk" that can occur between broad directional elements. The Hough transform also has the feature that it is very robust to the addition of random data that arise from poor image segmentation, since random image points are very unlikely to contribute coherently to a single point in the parameter space and will only add a low level of background counts.

The main drawback of the Hough transform is that it is usually performed on binary images and is thus dependent on the binarisation method that is used in segmenting the image[47]. The implementation proposed in this paper will avoid this drawback by performing a modified version of the Hough transform that uses concepts from the Radon transform to obtain a Hough/Radon transform without resorting to the information-losing binarisation step.

3. Quantitative directional analysis using the Hough and the Radon transforms

In this section we shall explain the steps in the Hough method of determining directional content in images. The image is first transformed into the Hough/Radon domain, while at the same time a second shadow domain is obtained which keeps a count of the number of pixels at a particular parameter point. The Hough/Radon-transformed image is filtered to obtain coherent peaks, and the filtered image is normalised to a value between 0.0 and 1.0. This normalisation procedure gives a relative weighting to the normal Hough transform. The shadow parameter space that contains the count of pixels that occupy a particular parameter cell is multiplied with this normalised parameter space to obtain a relative count of the number of pixels in the particular parameter cell. The shadow parameter space is then integrated in each angle band to obtain a count of the number of pixels that occupy each angle.

3.1. *The Hough and Radon transforms*

Deans[48] showed that there is a direct relationship between the Hough and Radon transforms. In fact, the Hough transform is a special case of the Radon transform but with a different transform origin, and performed only on a binary image. The Radon transform has its transform origin at the centre of the original image whereas the Hough transform has its transform origin at the location of the image where the row and column indices are zero. Thus distances, ρ, that are calculated from equation 2 for a 256×256 image for the Hough transform would be calculated relative to the (0, 0) point in the original image, whereas for the Radon transform, the ρ values would be calculated relative to the (128, 128) point. A comparison between the operations of the two transforms on a line is shown in figure 2. From this figure we can see that the (ρ, θ) of the Hough transform are offset by a constant amount for all points in relation to the Radon transform variables (ρ', θ'). This difference between the two transforms affects the aggregation of collinear points in each domain. In the Radon domain, collinear peaks are more circular in nature due to the symmetric calculation of the distance ρ, while in the Hough domain the collinear points are more elliptical due to the asymmetric nature of ρ. Since the filter that we will be using to detect peaks was designed to detect asymmetric peaks in the Hough domain, we will be using the Hough domain for transformation of the image; however, we will be performing the Radon transform at each point in this space to obtain the peak information without use of a threshold level.

We calculate the Hough/Radon hybrid transform by updating the (ρ_i, θ_i) parameter point by adding the pixel intensity and not by incrementing by one as with the Hough transform. In this sense, brighter lines correspond to brighter peaks in the Hough domain. Performing the Hough/Radon transform in this manner also allows us to maintain the structure of the Hough domain so that a filtering step (to be described later in section 3.2) can be performed to detect peaks in the Hough domain.

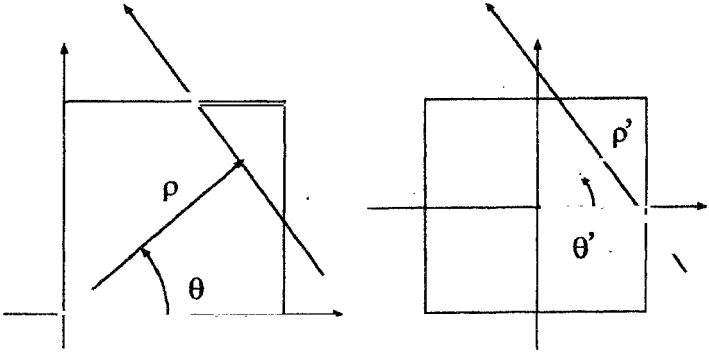

FIG. 2. Comparison between the Hough and Radon transform mappings.

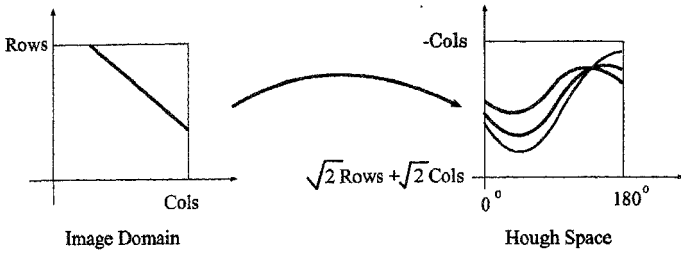

FIG 3. Hough/Radon transform mapping from the image space to the transform space.

The Hough/Radon transform of the image is indexed in the column space from 0° to 180°, and if *Rows* and *Cols* are the number of rows and columns in the input image, respectively, then the row space of the transform image is from $-Cols$ at the top of the image to $\sqrt{2}Rows+\sqrt{2}Cols$. An example of the mapping is shown in figure 3.

The generation of the Hough/Radon domain produces relative intensities of the directional nature of images, an example of which is shown in figure 4(b) for the synthetic test image "Test-1" shown in figure 4(a). However, the objective in this work is to obtain the number of pixels or the percentage of the picture as a whole which can be binned into a particular angle band. Therefore, it is necessary to form a shadow parameter space that keeps a count of the number of pixels that are in a particular cell in the parameter space. This shadow parameter space is the Hough transform of the image with no accompanying threshold level.

It is necessary to form both the Hough/Radon transform space as well as the Hough transform shadow space, since performing only the Hough transform on an unthresholded image will produce, for most images, a transform with little information about the image. Computing the shadow parameter space is the same as performing the Hough transform on a thresholded image for all pixels with a grey level greater than zero. The Hough/Radon transform, however, gives more differentiation between light and dark regions in an image, thus retaining all the information about the image while still performing the desired transform. The Hough transform is needed for later processing since we want a count of the number of pixels regardless of the intensity.

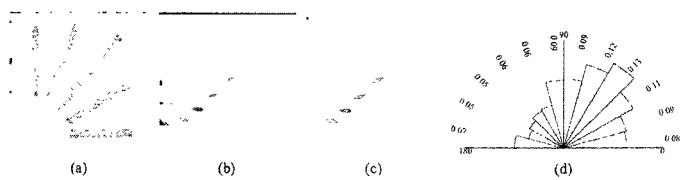

FIG. 4. (a) Test-1 image, (b) Hough/Radon transform, (c) Filtered transform, (d) Rose diagram.

From the image shown in figure 4(b) we can see the high level of "crosstalk" in the upper right quadrant. From figure 3, we see that this section maps to about the 100° to 165° angle band. This is due to the Hough transform's tendency to identify lines in an image even though the lines may not be directly connected. This is both a strength and a weakness of this method as we shall see later. The filtering procedure described in the following section will minimise this effect; however, it will still bias the results in some of the images.

3.2. *Peak detection through filtering*

While the Hough/Radon transform is a powerful way of determining the directional elements in an image, it lacks, by itself, any means by which to eliminate elements that do not contribute coherently to a particular directional pattern. This is due to the transform being performed on all points in an image, and hence simple integration along any column of the transform space will include all the points in the image. A second step is needed to eliminate those pixels that do not contribute significantly to a particular pattern. Leavers and Boyce[49] used the Radon transform to generate a simple 3×3 filter to locate maxima in the Hough transform space which correspond to connected collinearities in an "edge image" space.

The filter is derived from the (ρ, θ) parameterisation of lines and the expected shape of the distribution of counts in the accumulator of the Hough transform space. For a linear element in an image, the shape is a characteristic "butterfly", which is a term commonly used to describe the characteristic falloff shape from a central accumulator point which corresponds to a line mapping in the Hough domain as shown in figure 3. It is shown by Leavers and Boyce[49] that for all lines in the image space, the extent of the corresponding butterfly for a line in the Hough domain is limited to one radian or approximately 58° of the central accumulator point.

The 2D filter

$$\begin{bmatrix} 0 & -2 & 0 \\ 1 & +2 & 1 \\ 0 & -2 & 0 \end{bmatrix} \tag{3}$$

has a high positive response to any distribution which has its largest value in the central pixel, falls off to approximately 50% on either side, and vanishes rapidly above and below the central pixel. This filter performs remarkably well in spite of having such a simple structure. The drawback is that it was designed for detecting lines of one pixel width. In the situation shown in figure 4(b), we can see that the broad directional components in the test image correspond to broad components in the Hough/Radon domain. This results in the filter of equation 3 detecting only the edges of the peaks in the Hough domain; an example of this is shown in figure 4(c).

The filter in equation 3 is also very sensitive to quantisation of the θ increments. This can be seen in the vertical streaks of intensity in figure 4(c). The vertical streaks occur at θ values that correspond to points where the value of ρ in equation 2 approaches an integral value. Increasing the spatial extent of the filter would reduce the sensitivity of the filter to noise as well as improve the ability of the filter to detect larger components in the Hough/Radon transform space. Detecting larger components in the Hough/Radon domain corresponds to detecting broad directional image components.

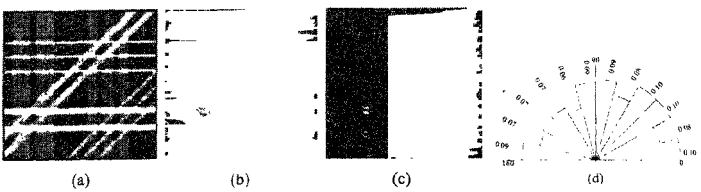

FIG 5 (a) Test-2 image, (b) Hough/Radon transform, (c) Filtered transform, (d) Rose diagram

Once the Hough/Radon transform has been filtered using the filter in equation 3, the resulting filtered image is normalised to the range of 0.0 to 1.0 and then multiplied, accumulator point by accumulator point, with the shadow Hough transform mentioned earlier. This step is performed in order to obtain the relative strength of the numbers of pixels at each of the detected peaks. This step also reduces accumulated quantisation noise from the Hough/Radon transformation and filtering steps. Peaks may be detected in a region of the Hough/Radon domain; however, there may be few corresponding pixels in the original image that map to these locations. Multiplying noisy peaks by areas that contain few points in the original image will reduce the final count of pixels in the corresponding angle bands.

3.3. *Integration*

The integration step is a trivial summation along each of the columns of the filtered parameter space. Since the Hough transform generates a parameter space which is indexed in the column space from 0° to 180°, each of the columns represents some fraction of a degree depending upon the quantisation interval selected for the transform. Also, since the Hough transform is a voting process, the peaks selected will contain some percentage of the pixels that are contained in the directional components.

4. Results

In selecting the test images, we have endeavored to obtain a broad selection images that have shading as well as images that have good foreground -- background separation, contrast, and depth of field. The first synthetically produced test image (Test-1) shown in figure 4(a) is the most simple of the test images, constisting of directional components that are clearly separated from the background of the image. The second synthetic test image (Test-2), shown in figure 5(a), consists of several surfaces that are oriented at four directions. The image contains a mixture of ramp and step edges as well as several surfaces of varying intensity that are occluded; it is a non-linear image in that the directional components do not add at the occluded locations.

The second pair of images shown in figure 6(a) (Bridge) and 7(a) (Forest) consists of natural scenes. The Bridge image is commonly used to test image processing algorithms; it contains a man-made object (the bridge), as well as various non-directional objects. The Forest image consists of trees which contain a multitude of small and large directional components at various directions. We have included these images to evaluate the performance of the algorithms with natural images including depth of field as well as undirected components.

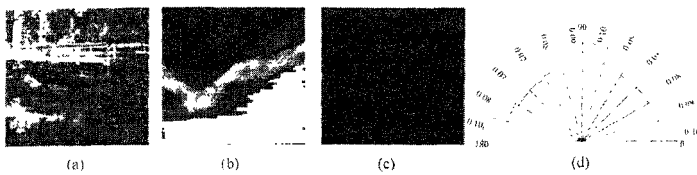

FIG. 6. (a) Bridge image, (b) Hough/Radon transform, (c) Filtered transform, (d) Rose diagram.

The images shown in figures 8(a) (Ligament-1) and 9(a) (Ligament-2) are examples of scanning electron microscope images of collagen fibers in rabbit medial collateral ligaments[1–4]. The Ligament-1 image is an example of ligament scar tissue, and the Ligament-2 image is an example of a normal ligament. It has been established that while normal ligaments have collagen fibers neatly aligned along the long axis of the ligament, scar tissues have an almost random distribution of the fibers.[1–4]

Figure 4 shows the results of the algorithm for the Test-1 image. In this image we can see the problem of the small-extent filter mentioned earlier in section 3.2. This filter detects only the edges of the transformed components and neglects the central section of each of these components. From the rose diagram[45, 1] shown in figure 4(d), we can see that the filter does detect the relative distribution of the linear components, that is, the petal at 45° should be about $\sqrt{2}$ times the size of the petals at 0° or at 90°; however, there is a large amount of smearing of the results which produces poor differentiation between the angle bands. We can also see from the rose diagram that there is a large amount of crosstalk detected in the 135° band where the output should be zero. This effect is probably due to a combination of crosstalk as well as quantisation noise from the Hough/Radon transform.

Figure 5 shows the results for the Test-2 image, where again we can see the difficulty this algorithm has in detecting large elements in the transform space. Figure 5(c) shows that the central sections of the detected peaks are not accentuated, which gives erroneous results. The petals in figure 5(d) at 90° should have been twice as large as the petals at 45° or 0°. Further, there is a lack of strong directional patterns in the 135° band, which is due to the attenuated nature of the corresponding elements in the original image. This indicates that the algorithm is performing directional assessment based upon the intensity of the elements as opposed to strict binning upon direction.

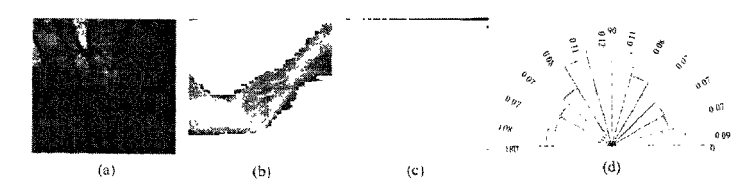

FIG. 7. (a) Forest image, (b) Hough/Radon transform, (c) Filtered transform, (d) Rose diagram.

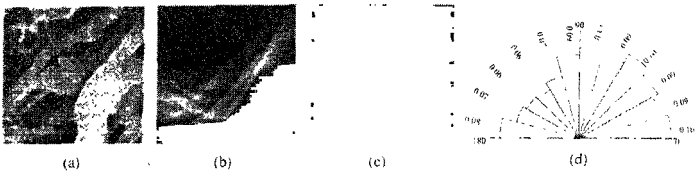

FIG. 8. (a) Ligament-1 image, (b) Hough/Radon transform, (c) Filtered transform, (d) Rose diagram.

From the results for the Bridge image (see figure 6) it is seen again that the algorithm is quantising upon intensity as well as directional orientation. This is apparent from the large petals in the 0° and 90° directions in figure 6(d), which correspond to the high-intensity components that exist in each of these angle bands.

For the Forest image shown in figure 7(a), we see from the results shown in figures 7(c) and 7(d) that the algorithm detects the strong vertical nature of the image. The algorithm performs well for this image mostly due to the strong intensity elements of the trees as well as the narrow extent of the tree elements. Since the tree branches are narrow in extent, the filter detects these elements as individual units and not as edges of larger linear segments.

For the ligament images shown in figures 8(a) and 9(a), the algorithm performs reasonably well, giving reasonable representational results for both of these images as shown in figures 8(b)–(d) and 9(b)–(d). These results could contain artifacts due to the previously-mentioned problem of the algorithm with broad directional components, since both of these images have broad directional components.

5. Conclusion

We have presented a method for detecting directional elements in images using the Hough transform method of selecting linear elements from images. The method uses a hybrid combination of the Radon transform in the Hough domain, and then subsequently filters the transformed image to obtain peaks in the Hough/Radon domain. The filtered transform space is then multiplied, accumulator point by accumulator point, with the unthresholded Hough transform data to reduce noise as well as to give an accurate representation of the image from the standpoint of binning pixels corresponding to a particular angle band. The Radon technique of

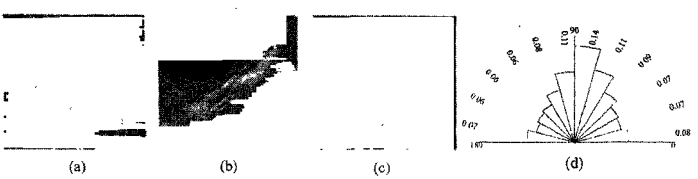

FIG. 9. (a) Ligament-2 image, (b) Hough/Radon transform, (c) Filtered transform, (d) Rose diagram.

summing pixel intensities is necessary to eliminate the need for thresholding. The technique of transforming the image into the Hough domain is needed in order to apply a filter designed in this domain to detect linear peaks. From the use of the Radon technique of summing intensities, the algorithm detects directional elements on the basis of intensity as well as orientation.

Further work is necessary to overcome limitations of the present algorithm, in particular in filtering in the Hough/Radon transform domain. The method should find use in analysis of ligament images[1–4] for studies on ligament injury, treatment, and healing.

Acknowledgements

This work was supported by grants from the Natural Sciences and Engineering Research Council (NSERC) of Canada.

References

1. CHAUDHURI, S., NGUYEN, H., RANGAYYAN, R. M., WALSH, S. AND FRANK, C. B., A Fourier domain directional filtering method for analysis of collagen alignment in ligaments. *IEEE Transactions on Biomedical Engineering*, 1987, **34(7)**, 509–518.

2. LIU, Z. Q., RANGAYYAN, R. M., AND FRANK, C. B., Directional analysis of images in scale–space, *IEEE Transactions on Pattern Analysis and Machine Intelligence*, 1991, **13(11)**, 1185–1192.

3. LIU, Z. Q., RANGAYYAN, R. M., AND FRANK, C. B., Statistical analysis of collagen alignment in ligaments by scale–space analysis, *IEEE Transactions on Biomedical Engineering*, 1991, **38(6)**, 580–588.

4. FRANK, C. B., MACFARLANE, EDWARDS, P., RANGAYYAN, R., LIU, Z.-Q., WALSH, S., AND BRAY, R., A quantitive analysis of matrix alignment in ligament scars: A comparison of movement versus immobilization in an immature rabbit model, *J. Orthopaedic Research*, 1991, **9(2)**, 219–227

5. JOHNSON, R. W., Characterization of fiber behavior in a nonwoven web through image analysis of tracer fibers, In *TAPPI Proceedings – 1988 Nonwovens Conference*, pp. 217–221, 1988. TAPPI Press.

6. VILLA, K. M. AND BUCHANAN, D. R., Image analysis and the structure of nonwoven fabrics, In *INDA-TEC. The International Nonwovens Technological Conference*, pp. 83–101, Philadelphia, PA, USA, June 1986. Association of the Nonwoven Fabrics Industry, New York, NY, USA

7. HALEY, C. S. AND LANDOLL, L. M., Image analysis of real and simulated nonwoven fabrics, In *INDA-TEC: The International Nonwovens Technological Conference*, pp. 65–82, Philadelphia, PA, USA, June 1986. Association of the Nonwoven Fabrics Industry, New York, NY, USA.

8. YUHARA, T., HASUIKE, M. AND MURAKAMI, K., Fibre orientation measurement with the two-dimensional power spectrum of a high-resolution soft x-ray image, *J. Pulp and Paper Science*, 1991, **17(4)**, J110–J114.

9. YANG, C. F., CROSBY, C. M., EUSUFZAI, A. R. K. AND MARK, R. E., Determination of paper sheet fiber orientation by a laser optical diffraction method, *J. Applied Polymer Science*, 1987, **34**, 1145–1157.

10. BRESEE, R. R. AND DONELSON, D. S., Small-angle light scattering for analysis of a single fiber, *J. Forensic Sciences*, 1980, **25(2)**, 413–422.

11. DZIEDZIC-GOCLAWSKA, A., ROZYCKA, R., CZYBA, J. C., SAWICKI, W., MOUTHER, R., LENCZOWSKI, S. AND OSTROWSKI, K., — Application of the optical Fourier transform for analysis of the spatial distribution of collagen fibers in normal and osteopetrotic bone tissue, *Histochemistry*, 1982, **74**, 123–137.

12 KOMORI, M., MINATO, K., NAKANO, Y., HIRAKAWA, Y. AND KUWAHARA, M., — Automatic measurement system for congenital hip dislocation using computed radiography. In *Medical Imaging II*, vol 914, pp. 665–668, Proceedings of the SPIE, 1988.

13 KUROGI, S., JIANQIANG, Y. AND MATSUOKA, K., — Measurement of the angle of rotated images using Fourier transform, *Transactions of the Institute of Electronics, Information and Communication Engineers*, 1990, *D-II*, J73D-II(4), 590–596.

14. DENSLOW, S., ZHANG, Z., THOMPSON, R. P. AND LAM, C. F., — Statistically characterized features for directionality quantitation in patterns and textures, Pattern Recognition, 1993, **26**, 1193–1205.

15. GONCHAROV, A. B. AND GELFAND, M. S., — Determination of mutual orientation of identical particles from their projections by the moments method, *Ultramicroscopy*, 1988, **25(4)**, 317–328.

16. ABRAMSON, S. B. AND FAY, F. S., — Application of multiresolution spatial filters to long-axis tracking, *IEEE Transactions on Medical Imaging*, 1990, **9(2)**, 151–158.

17. ENG, K., RANGAYYAN, R. M., BRAY, R. C., FRANK, C. B., ANSCOMB, L. AND VEALE, L., — Quantitative analysis of the fine vascular anatomy of articular ligaments, *IEEE Transactions on Biomedical Engineering*, 1992, **32**, 546–551.

18. BRAY, R. C., RANGAYYAN, R. M. AND FRANK, C. B., — Normal and healing ligament vascularity: a quantitative histological assessment in the adult rabbit medial collateral ligament, *J Anatomy*, 1996, **188**, 87–95.

19. KRONICK, P. L. AND SACKS, M. S., — Quantification of vertical-fiber defect in cattle hide by small-angle light scattering, *Connective Tissue Research*, 1991, **27**, 1–13.

20. SACKS, M. S. AND CHUONG, C. J., — Characterization of collagen fiber architecture in the canine diaphragmatic central tendon, *J. Biomechanical Engg*, 1992, **114**, 183–190.

21. PETROLL, W. M., CAVANAGH, H. D., BARRY, P., ANDREWS, P. AND JESTER, J. V., — Quantitative analysis of stress fiber orientation during corneal wound contraction, *J. Cell Science*, 1993, **104**, 353–363.

22. THACKRAY, B. D. AND NELSON, A. C., — Semi-automatic segmentation of vascular network images using a rotating structural element (ROSE) with mathematical morphology and dual feature thresholding, *IEEE Trans. Medical Imaging*, 1993, **12(3)**, 385–392.

23. EMBREE, P. AND BURG, J. P., — Wide-band velocity filtering – the pie slice process, *Geophysics*, 1963, **28**, 948–974.

24. TREITEL, S., SHANKS, J. L. AND FRASIER, C. W., — Some aspects of fan filtering, *Geophysics*, 1967, **32**, 789–806.

25. BEZVODA, V., JEŽEK, J. AND SEGETH, K., — FREDPACK- A program package for linear filtering in the frequency domain, *Computers & Geosciences*, 1990, **16(8)**, 1123–1154.

26. RAO, A. R., — *A Taxonomy for Texture Description and Identification*, Springer-Verlag, New York, NY, 1990.

27. JACOBBERGER, P. A., — Mapping abandoned river channels in Mali through directional filtering of thematic mapper data, *Remote Sensing of Environment*, 1988, **26(2)**, 161–170.

28 ARSENAULT, H. H., SHOUIK, M. K. AND BROUSSEAU, N., Optical filtering of aeromagnetic maps, *Applied Optics*, 1974, **13**, 1013–1017

29. MOORE, G. K. AND WALTZ, F. A., Objective procedures for lineament enhancement and extraction, *Photogrammetric Engineering and Remote Sensing*, 1983 **49(5)**, 641–647

30 DUVERNOY, J. AND CHALASINSKA-MACUKOW, K., Processing measurements of the directional content of Fourier spectra, *Applied Optics*, 1981, **20(1)**, 136–144.

31. DUGGIN, M., ROWNTREE, R. A. AND ODELL, A. W., Application of spatial filtering methods to urban feature analysis using digital image data, *International Journal of Remote Sensing*, 1988, **9(3)**, 543–553.

32. CARRERE, V., Development of multiple source data processing for structural analysis at a regional scale, *Photogrammetric Engineering and Remote Sensing*, 1990, **56(5)**, 587–595

33 SHLOMOT, E., ZELVI, Y., AND PEARLMAN, W. A., The importance of spatial frequency and orientation in image decomposition and coding, In *Visual Communication and Image Processing*, vol. 845, pp 152–158, Proceedings of SPIE, 1987.

34 LI, H. AND HE, Z., Directional subband coding of images, In *International Conference on Acoustics, Speech, and Signal Processing*, vol. III, pp 1823–1826, Glasgow, Scotland, May 1989. IEEE, Acoustics, Speech and Signal Processing Society.

35 IKONOMOPOULOS, A., AND KUNT, M., Directional filtering, zero crossing, edge detection and image coding, In H. W. Schussler, editor, *Signal Processing II: Theories and Applications*, pp. 203–206 Elsevier, New York, 1983.

36. KUNT, M., IKONOMOPOULOS, A. AND KOCHER, M., Second generation image coding techniques, *Proc. of the IEEE*, 1985, **73**, 549–574.

37. IKONOMOPOULOS, A AND KUNT, M., High compression image coding via directional filtering, *Signal Processing*, 1985, **8**, 179–203

38. KUNT, M., Recent results in high-compression image coding, *IEEE Transactions on Circuits and Systems*, 1987, **CAS-34**, 1306–1336

39 HOU, H. S. AND VOGEL, M. J., Detection of oriented line segments using discrete cosine transform, In *Intelligent Robots and Computer Vision: Seventh in a Series*, 1988, vol. 1002, pp. 81–87, *Proc. of SPIE*.

40 DUDA, R. O. AND HART, P. E., Use of the Hough transformation to detect lines and curves in pictures, *Communication of the ACM*, 1972, **15(1)**, 11–15.

41. BALLARD, D. H., Generalizing the Hough transform to detect arbitrary shapes, *Pattern Recognition*, 1981, **13**, 111–122.

42. ILLINGWORTH, J. AND KITTLER, J., The adaptive Hough transform, *IEEE Trans. Pattern Analysis and Machine Intelligence*, 1987, **9**, 690–698.

43 ILLINGWORTH, J. AND KITTLER, J., A survey of the Hough transform, *Computer Vision, Graphics, and Image Processing*, 1988, **44**, 87–116.

44. PRINCEN, J., ILLINGWORTH, J. AND KITTLER, J., A formal definition of the Hough transform: properties and relationships, *J. Math. Vis.*, 1992, **1**, 153–168.

45. ROLSTON, W. A., Directional image analysis, Master's thesis, The University of Calgary, Calgary, Alberta, Canada, April 1994.

46. EICHMANN, G. AND KASPARIS, T., Topologically invariant texture descriptors, *Computer Vision, Graphics, and Image Processing*, 1988, **41**, 267–281.

47. SHAPIRO, V. A., On the Hough transform of multi-level pictures, *Pattern Recognition*, 1996, **29(4)**, 589–602.

48. DEANS, S. R., Hough transform from the Radon transform, *IEEE Transactions on Pattern Analysis and Machine Intellegence*, 1981, **3**, 185–188.

49. LEAVERS, V. F. AND BOYCE, J. F., The Radon transform and its applicaton to shape parameterization in machine vision, *Image and Vision Computing*, 1987, **5**, 161–166